Pbx1 is required for adult SVZ neurogenesis

Britta Moyo Grebbin[1,4], Ann-Christin Hau[1,5], Anja Groß[1], Marie Anders-Maurer[1], Jasmine Schramm[1,6], Matthew Koss[2,7], Christoph Wille[1,8], Michel Mittelbronn[1], Licia Selleri[2,3], and Dorothea Schulte[1,‡]

[1] Institute of Neurology (Edinger Institute), J. W. Goethe University Medical School, German Cancer Consortium (DKTK), Heinrich-Hoffmann Str. 7, D-60528 Frankfurt, Germany

[2] Department of Cell and Developmental Biology, Weill Medical College of Cornell University, 1300 York Avenue, New York, NY 10065, USA

[3] Program in Craniofacial Biology, Institute of Human Genetics, Eli and Edythe Broad Center of Regeneration Medicine & Stem Cell Research, Departments of Orofacial Sciences and Anatomy, University of California, San Francisco, 513 Parnassus Avenue, HSW 710, San Francisco, CA 94143

[4] present address: Georg-Speyer Haus and German Cancer Consortium (DKTK), Paul-Ehrlich-Straße 42-44, D-60596 Frankfurt, Germany

[5] present address: Luxembourg Institute of Health, 84 Val Fleuri, L-1526 Luxembourg

[6] present address: Dr. Ehrlich Pharma, D-88410 Bad Wurzach, Germany

[7] present address: Regeneron Pharmaceuticals, Inc., Tarrytown, NY 10591, USA

[8] present address Department of Internal Medicine I, University Clinic Ulm, Albert-Einstein-Allee 23, D-89081 Ulm, Germany

‡ Author for correspondence   tel: ++49-(0)69-6301-84159

fax: ++49-(0)69-6301-84150

email: dorothea.schulte@kgu.de

Key words: TALE-homeodomain protein, adult neurogenesis, subventricular zone, cell fate specification, doublecortin, pioneer factor

Author contributions

B.M.G. designed and conducted the experiments and contributed to writing the manuscript; A.C.H. and A.G. contributed to Figs. 7 and 8, M.A.M. to Figs. 1, 6 and S3, J.S. to Fig. 1, C.W. to Figs. 1 and S1, M.M. contributed to Fig. S2 and helped with experiments related to Fig. 6; M.K. and L.S. generated the mouse models used and shared them before their publication, and contributed to writing the manuscript; D.S. designed the study, discussed and supervised the experiments, and wrote the manuscript.

ABSTRACT

TALE-homeodomain proteins function as part of heteromeric complexes that contain one member each of the PBC- and MEIS/PREP-subclasses. As we have recently shown, MEIS2 cooperates with the neurogenic transcription factor PAX6 in the control of adult subventricular zone (SVZ) neurogenesis in rodents. Expression of the PBC-protein *Pbx1* in the SVZ has been reported but its functional role(s) had not yet been investigated. Using a genetic loss-of-function model, we now show that *Pbx1* is an early regulator of SVZ neurogenesis. Targeted deletion of *Pbx1* by retroviral transduction of Cre recombinase into *Pbx2*-deficient SVZ stem- and progenitor cells carrying floxed alleles of *Pbx1* significantly reduced the production of neurons and increased the generation of oligodendrocytes. Loss of *Pbx1*-expression in neuronally committed neuroblasts in the rostral migratory stream in a *Pbx2* null (*Pbx2*$^{-/-}$) background, by contrast, severely compromised cell survival. By chromatin immunoprecipitation from endogenous tissues or isolated cells, we further detect PBX1 binding to known regulatory regions of the neuron-specific genes *DCX* and *TH* days or even weeks before the respective genes are expressed during the normal program of SVZ neurogenesis, suggesting that PBX1 may act as priming factor to mark these genes for subsequent activation. Collectively, our results establish that PBX1 regulates adult neural cell fate determination in a way that goes beyond the that of its heterodimerization partner MEIS2.

INTRODUCTION

The SVZ of the lateral ventricle walls is one of the adult neurogenic niches in the adult rodent brain capable of generating neurons in a non-pathological context. Multipotent neural stem cells of the SVZ produce transient amplifying progenitors (TAPs), which predominantly generate neuroblasts *in vivo*. Adult neural stem cells are subsets of SVZ astrocytes, defined by their characteristics of self-renewal and multipotency, while TAPs and neuroblasts can be easily distinguished on the basis of specific marker gene expression. TAPs, for instance, express the basic helix-loop-helix (bHLH) transcription factor *achaete-scute family transcription factor 1* (*Ascl1*; *Mash1*), while neuroblasts can be recognized by their expression of *Doublecortin* (*DCX*), *neuronal βIII-tubulin* (*Tubb3*; *TuJ1*) or polysialylated-NCAM (PSA-NCAM). Neuroblasts migrate along the rostral migratory stream (RMS) into the olfactory bulb (OB), where they differentiate into a wide variety of inhibitory neuron phenotypes, including GABA-ergic granule cells (GCs) or dopaminergic, calbindin- or calretinin- expressing periglomerular interneurons (PGNs), and thus contribute to a continuous neuronal turn-over in the adult OB (Lim and Alvarez-Buylla, 2014). Defective replacement of OB interneurons has been implicated in impaired olfaction-related behavior, whereas excessive proliferation in the SVZ has been linked to the formation of glial tumors (Sakamoto et al., 2014; Barami et al., 2009). Adult SVZ neurogenesis therefore needs to be tightly regulated in order to maintain a proper balance between self-renewal and differentiation towards neuronal or glial lineages.

Pre B-cell leukemia homeodomain (PBX) transcription factors constitute the PBC-subgroup of TALE (three amino acid loop extension) homeodomain (HD) containing proteins. PBX transcription factors are essential regulators of embryonic development. They contribute to the correct patterning of the anterior-posterior body axis, confer regional identity and are involved in the regulation of proliferation, apoptosis and differentiation (Berkes et al., 2004; Ferretti et al., 2011; Gordon et al., 2011; Koss et al., 2012; Yao et al., 2013). *Pbx1* participates

in many developmental processes, as demonstrated by the complex phenotypes associated with *Pbx1* loss-of-function in mice (Brendolan et al., 2005; DiMartino et al., 2001; Ferretti et al., 2011; Golonzhka et al., 2015; Koss et al., 2012; Manley et al., 2004; Selleri et al., 2001; Stankunas et al., 2008; Vitobello et al., 2011). Genes encoding *PBC*-class HD proteins share a high degree of sequence homology and have overlapping functions in domains of co-expression *in vivo* (Capellini et al., 2011). In fact, select developmental defects associated with *Pbx1* loss-of-function were only uncovered when the *Pbx1* deficiency was combined with homozygous or heterozygous loss of *Pbx2* or *Pbx3* (Capellini et al., 2011; Ferretti et al., 2011; Koss et al., 2012). Mechanistically, PBX1 associates with members of the MEIS/PREP-subclass of TALE-HD proteins, but can also form heteromeric complexes with HOX-proteins, non-HOX HD-containing proteins, bHLH- or PAX-proteins (Ladam and Sagerström, 2014; Longobardi et al., 2014; Schulte 2014). As we have recently shown, MEIS2 is an essential co-factor of the neurogenic transcription factor PAX6 and as such required for the acquisition of a general neuronal fate in the SVZ and the subsequent differentiation of a subpopulation of these cells towards dopaminergic periglomerular neurons (Agoston et al., 2014; Brill et al., 2008; Hack et al., 2005; Kohwi et al., 2005; Kohwi et al., 2007). *Pbx1* expression in structures associated with adult forebrain neurogenesis in rodents has been reported, but its functional relevance has remained as yet unresolved (Redmond et al., 1996).

RESULTS

Pbx1, Pbx2 and *Pbx3* exhibit distinct expression patterns in the adult SVZ

We first characterized *Pbx1* mRNA expression and protein localization in the brain of 7-11 week old mice. Groups of cells staining positive for *Pbx1* transcripts and protein were located directly underneath the ependymal cell layer (EpCL) at the dorsal and lateral walls of the SVZ (Fig. 1A-F). Cells exhibiting nuclear immunoreactivity for PBX1 contribute to the Ki67^{+}, rapidly proliferating cell population in the SVZ, with 65.4% (± 5.5%) of the Ki67^{+} cells also labeling for PBX1 (Fig. 1D, H; Table S3). Consistent with expression in TAPs, we found that 96.6% (± 5.4%) of the *ASCL1*-expressing cells in the adult SVZ label for PBX1 (Fig. 1E, H; Kim et al., 2007). The gene encoding the intermediate filament protein Nestin is expressed in ependymal cells, TAPs and slowly proliferating bona fide neural stem cells (Cattaneo and McKay, 1990; Lendahl et al., 1990). Nestin^{+} cells in the subependyma, but not the EpCL itself, were also immunopositive for PBX1, further strengthening the notion that PBX1 protein is present in neural progenitor cells of the adult SVZ (Fig. 1F). Of the *TuJ1*-expressing neuroblasts in the SVZ or RMS, 81.75% (± 13.2%) were immunoreactive for PBX1 and virtually all of these co-labeled for MEIS2 (Fig. 1G-I; Agoston et al., 2014). Notably, the dentate gyrus of the hippocampus, the second major stem cell niche in the adult mouse brain, is devoid of Pbx1 transcripts or protein (Fig. 1J, K). Similar to *Meis2*, *Pbx1*-expression thus specifically marks the SVZ neurogenic niche (Agoston et al., 2014). By contrast, almost all cells in the adult SVZ, RMS, corpus callosum, cortex, and striatum stained positive for PBX2, consistent with the wide-spread expression of *Pbx2* in the embryo (Fig. 1L-M, Fig. S1; Selleri et al., 2004). Only few cells in the SVZ and RMS expressed *Pbx3* and these were mostly immunonegative for PBX1 or MEIS2 (Fig. 1N-O"). Double-labeling for each of the three *Pbx*-encoding genes together with MEIS2 established that virtually all MEIS2-expressing cells stained positive for PBX1 and PBX2, whereas only 13.9% of the MEIS2^{+} cells were immunoreactive for PBX3 (Fig. 1P).

In the OB, PBX1-immunoreactive cells contribute to GCs and PGNs, with virtually all GCs and on average 22.8% of the calbindin[+], 23.65% of the calretinin[+] and 94.46% of the dopaminergic, tyrosine hydroxylase[+] (TH)[+] PGNs labeling for PBX1 (Fig. 2A-G, S2; Table S3). PBX3 was absent from the TH[+] PGN subtype (Fig. 2H, S2). Collectively the *Pbx1*-expression profile suggests an early role for PBX1 in neuronal lineage specification in the SVZ and a later contribution to the adult generation of OB interneurons.

Targeted deletion of *Pbx1* in adult SVZ-derived progenitor cells induces a neurogenic to oligodendrogliogenic fate change *in vitro* and *in vivo*

The neurosphere assay allows the propagation of adult neural stem cells and TAPs in the presence of EGF and FGF2 *in vitro* while maintaining their multipotency at least at early passages in culture (Reynolds and Weiss 1992; Weiss et al., 1996; Rietze and Reynolds, 2006). Free-floating adult neurospheres (aNS) mostly consist of rapidly proliferating TAPs as well as a smaller number of presumably activated and EGF-responsive stem cells, both of which express *Nestin* (Pastrana et al., 2009, 2011). Consistent with the prominent expression of *Pbx1* in TAPs *in vivo*, PBX1 was detected in most Nestin^{+} aNS cells (aNS; Fig. 3A). To distinguish between TAPs and neural stem cells, we labeled aNS with the green fluorescent cytoplasmic dye 5-Carboxyfluorescein Diacetate, Acetoxymethyl Ester (CFDA AM; Fig. 3B-E). When applied to free-floating aNS, the CFDA-label is quickly diluted out by cell division in TAPs, but retained in the more quiescent stem cells, which are visible as brightly labeled cells positioned in the center of large aNS (arrow in Fig. 3C). Intense nuclear staining for PBX1 was seen in 98.3% of the CFDA-negative, Nestin[+] TAPs, but in only 4% of the CFDA-label-retaining, Nestin[+] putative SVZ-stem cells (Fig. 3D, E). Upon growth factor withdrawal and plating on appropriate substrates, aNS will differentiate into neurons, astroglia or oligodendrocytes (Doetsch et al., 2002; Reynolds and Weiss, 1992). When we induced SVZ-derived aNS to differentiate on laminin, PBX1 protein was retained in newborn *TuJ1-*

expressing neurons and GFAP$^+$ astrocytes but lost from oligodendrocytes (immunoreactive for the O4 antigen) (Fig. 3F-I and Table S3).

To investigate whether *Pbx1* has a role in neural cell fate specification, we used a conditional allele of *Pbx1* (*Pbx1*$^{fl/fl}$) that allows Cre-mediated deletion of exon 3 of the *Pbx1* gene (Koss et al., 2012). PBX1 immunoreactivity was lost within 48 hours when aNS derived from *Pbx1*$^{fl/fl}$ mice were infected with retroviruses carrying Cre-recombinase together with an IRES-GFP cassette (Cre-GFP; Fig.4A, B). Upon differentiation, Cre-GFP transduced, *Pbx1*-deficient aNS cultures generated neurons and astrocytes at frequencies comparable to cultures transduced with GFP alone (Fig. S3). We therefore considered the possibility of functional compensation. Because PBX2 co-localizes with PBX1 in the SVZ (Fig. 1) and is known to compensate for loss of *Pbx1* in embryonic domains of co-expression, we crossed the conditional *Pbx1*-mutant strain to a mouse line homozygous mutant for *Pbx2* to obtain Pbx1$^{fl/fl}$;Pbx2$^{-/-}$ compound mutant animals (Capellini et al., 2011; Ferretti et al., 2011; Koss et al., 2012; Selleri et al., 2004). Mice with a constitutive knockout of *Pbx2* are viable and show no obvious phenotype (Selleri et al., 2004). Absence of PBX2 protein in homozygous *Pbx2* mutant animals was confirmed *in vivo* and in aNS cultures derived from these animals *in vitro* by immunohistochemical staining and Western Blot analysis (Fig. S4). Similar to aNS cultures lacking *Pbx1*, cultures obtained from *Pbx2*-single mutant animals did not show defective neurogenesis or gliogenesis, as did cultures obtained from animals of different heterozygous mutant genotypes (Fig. S3). We therefore transduced aNS from homozygous *Pbx1*$^{fl/fl}$;*Pbx2*$^{-/-}$ animals with Cre-GFP expressing virus to induce loss of *Pbx1* on a *Pbx2*-deficient background (termed 'double knock-out' (dKO) hereafter). *Pbx1*$^{fl/fl}$;*Pbx2*$^{-/-}$ cells infected with viruses that express only GFP served as control (single KO for *Pbx2*, 'sKO'). Upon differentiation, generation of neurons from dKO progenitor cells was significantly reduced compared to sKO control cells (Fig. 4C, E). This was paralleled by an increased production of cells of the oligodendroglial lineage, evident in a sharp rise in the number of

cells expressing the oligodendrogliogenic transcription factor Olig2 or the O4-antigen, a marker for mature oligodendrocytes (Fig. 4D, E). By contrast, the number of astrocytes generated from dKO and sKO progenitors did not differ (Fig. 4E, Table S4).

We next injected Cre-GFP- or GFP-expressing retroviruses into the SVZ of $Pbx1^{fl/fl}$;$Pbx2^{-/-}$ mice *in vivo*. We first confirmed efficient loss of PBX1 protein in Cre-GFP transduced cells, observing successful elimination in 97.25% of the Cre-expressing cells three days after virus injection (Fig. 5A-C). Like *in vitro*, retroviral transduction of Cre-recombinase reduced the relative proportion of DCX^+ or PSA-NCAM$^+$ neurons and enhanced the proportion of OLIG2-immunoreactive oligodendrocyte precursor cells (Fig. 5D-L, Table S4). Because oligodendrocyte precursor cells originating from the dorsal SVZ migrate into the overlying corpus callosum or the laterally located white matter tracks of the striatum instead of entering the RMS, we mapped the distribution of sKO and dKO cells in brain sections obtained 3 days after injection of GFP or Cre-GFP expressing retroviruses into the SVZ (Menn et al., 2006). Notably, dKO cells more frequently populated the corpus callosum and were found less frequently in the SVZ and RMS than sKO cells (Fig. 5M-O). Loss of *Pbx1*-expression in adult neural progenitor cells thus alters the gene expression profile and migratory behavior of the cells. Collectively, these results implicate *Pbx1* in the regulation of neurogenic versus oligodendrogliogenic cell fate decisions of adult SVZ progenitor cells.

Loss of *Pbx1* during late stages of differentiation compromises cell survival

PBX-family proteins can form stable heterodimers with MEIS proteins (Ladam and Sagerström, 2014). In the SVZ-OB neurogenic system, MEIS2 together with PAX6 (and the *distal-less*-homologue DLX2), is necessary for the acquisition of a dopaminergic PGN fate (Agoston et al., 2014; Brill et al., 2008; Hack et al. 2005; Kohwi et al., 2005). Therefore, we first examined whether PBX1 participates in the formation of higher order MEIS2/PAX6 containing transcriptional complexes. Indeed, PBX1-specific antibodies successfully

precipitated both proteins from OB extracts (Fig. S5). To test whether *Pbx1* also has a role in dopaminergic PGN differentiation, we stereotactically injected GFP- or Cre-GFP- expressing retroviruses into the rostral RMS, where dopaminergic neurons of the OB undergo their final mitosis (Hack et al., 2005). Because dopaminergic PGNs are characterized by a particularly slow maturation, the mice were analyzed up to 60 days post injection. It was previously reported that genetic ablation of *Pax6* by a similar experimental approach, or forced expression of function-blocking forms of PAX6 or MEIS2 in neuroblasts of the RMS, elicited a cell fate change from dopaminergic to calretinin-expressing PGNs (Agoston et al., 2014; Hack et al., 2005; Kohwi et al., 2005). To our surprise, only few dKO cells could be recovered from Cre-GFP-infected *Pbx1*^{fl/fl};*Pbx2*^{-/-} brains, whereas sKO cells were abundant in the granule cell layer (GCL) and glomerular layer (GL) of GFP-infected littermates (Fig. 6A-C). To more closely compare the survival of sKO and dKO cells, we performed simultaneous lineage tracing of both genotypes in the same animal (Fig. 6D-G). For this purpose, equal-titer retroviral stocks expressing either tdTomato or Cre-GFP were mixed and injected into the rostral RMS of *Pbx1*^{fl/fl};*Pbx2*^{-/-} animals. Ten days post injection, many red-fluorescent (sKO) and green-fluorescent (dKO) cells were seen in the core of the OB, where the migratory stream of SVZ-born neuroblasts enters the OB (Fig. 6D). At 21 days post injection, both sKO and dKO cells were found dispersed throughout the GCL, and some sKO cells had settled in the GL (Fig. 6E). We then followed the survival and migration of sKO and dKO cells by assessing their frequency and distribution at 19, 21, 28, 35, and 50 days post injection. Previous BrdU birthdating experiments had shown that only a fraction of the neuroblasts that leave the SVZ can successfully integrate into the OB circuitry and survive for longer than one month (Petreanu et al., 2002; Winner et al., 2002). In agreement with these studies, we observed a continuous, gradual decline in the total number of tdTomato-labeled sKO cells during the 31 days of our analysis (Fig. 6F, left). Interestingly, the total number of dKO cells decreased even more sharply, with only very few cells still present in the OB at 50 days post

injection (Fig. 6F, right). When we grouped the cells according to their location in the OB, the relative distribution of sKO in the GCL, plexiform layer and GL suggested that equal proportions of the surviving cells entered the GL or remained in the GCL, with a transient population of cells found in the plexiform layers, likely entering them on their way to the GL (Fig. 6F, G, left panel each). By contrast, dKO cells were never observed in the GL (Fig. 6F, G, right panel each). Because apoptotic cell death is a common feature of regions of ongoing neurogenesis in the brain, including the adult OB, we quantified the proportion of tdTomato$^+$ or Cre-GFP$^+$ cells that co-stained with an antibody against cleaved (activated) caspase-3 (ac-caspase3) (Biebl et al., 2000; Winner et al., 2002). We found that between 1.2% and 1.5% of the dKO cells were ac-caspase3$^+$ in the RMS at 3, 7, and 10 days post injection. Notably, 5.8% of the dKO cells in the GCL were ac-caspase3$^+$ at 28 and 35 days post injection. By contrast, apoptosis never occurred in sKO cells within the RMS and reached only 3.5% in the GCL and GL 35 days post injection. *Pbx1* is thus required for the long-term survival of adult born OB neurons. Considering that dopaminergic PGNs are PBX1-immunoreactive (Fig. 2), it was unexpected to detect TH$^+$ dKO cells 60 days post injection (Fig. 6H). These cells likely survived as a result of ectopic upregulation of PBX3, since sKO in the OB were mostly PBX3-negative, whereas 75% of the dKO cells expressed *Pbx3* (Fig. 6I-K). Given the high degree of homology shared between PBX1, PBX2 and PBX3, PBX3 may indeed functionally replace PBX1 in the regulation of genes required for dopaminergic differentiation in dKO cells.

PBX1 binding to the *DCX*-promoter/enhancer precedes *DCX*-expression

DCX and *TH* are genes regulated jointly by MEIS2 and PAX6. As we previously showed by chromatin immunoprecipitation followed by quantitative PCR (ChIP-qPCR), a MEIS/PBX consensus site located 2725 bp upstream of the start codon of the murine *DCX*-gene (*DCXI*) is bound by MEIS2, PAX6 and the PAX6-interacting transcription factor DLX2 in neuroblasts

(Agoston et al., 2014). Moreover, the endogenous *DCX*-promoter/proximal enhancer (Karl et al., 2005; Piens et al., 2010); NCBI AY590498, BX530055) is transcriptionally activated by MEIS2 and PAX6 (Agoston et al., 2014). In *in vitro* generated neurons, a PBX1-specific antibody efficiently precipitated the *DCXI* chromatin fragment (Fig. 7B). Reflecting the robust expression of *DCX* in these cells, the *DCXI* site carried the H3K4^{me3} epigenetic mark, which is associated with active promoters (Fig. 7C; (Barski et al., 2007)). PBX1 also induced expression of a DCX-promoter/enhancer-driven luciferase reporter in HEK293T cells, both alone (likely owing to low level endogenous *Meis/Prep*-expression in these cells) and together with ectopically expressed MEIS2 (Fig. 7D). By contrast, a reporter in which the MEIS/PBX consensus site was deleted could not be stimulated by transfection of *Pbx1* and *Meis2* (Fig, 7E). Interestingly, we found that PBX1 was already bound to the DCXI site in aNS, even though these cells do not yet express *DCX* (Fig. 7F). In aNS, the *DCXI* genomic region lacked H3K4^{me3}- and H3K27^{me3} epigenetic marks, indicative of a transcriptionally non-restricted chromatin state (Fig. 7G). The PBX1-specific antibody was ineffective in ChIP assays on the *DCXI* site in *in vitro* differentiated astroglia or on a validated PBX-binding site within the promoter of myogenin in aNS (Fig. 7H (Berkes et al., 2004)). In addition, siRNA mediated knock-down of *Pbx1* effectively reduced PBX1 binding to the *DCXI* site in aNS, further confirming the specificity of the PBX1 antibody that was used in the ChIP experiments (Fig. S6). Together, these results identify PBX1 as transcriptional activator of the *DCX*-promoter/enhancer and show that PBX1, in contrast to MEIS2, associates with the *DCXI* site already prior to *DCX*-expression.

PBX1 binds a known regulatory region of the *TH*-gene already in progenitor cells

We also examined whether PBX1 binds a known TALE-HD binding site, *THI*, 3479 bp upstream of the start codon of the mouse *TH*-gene within a published promoter/proximal enhancer. In a previous study, ChIP analysis with a MEIS2-specific antibody and chromatin

prepared from adult mouse OB showed enrichment of MEIS2 at this motif (Fig. 8A; NCBI AF415235; (Agoston et al., 2014)). ChIP-qPCR experiments with the PBX1-specific antibody precipitated the *THI* genomic fragment from freshly isolated OB or SN4741 cells, a dopaminergic neural progenitor cell line derived from mouse embryonic substantia nigra (Fig. 8B-D; (Son et al., 1999)). PBX1 thus binds the *THI* site in *TH*-expressing cells. Interestingly, ChIP-qPCR experiments from primary aNS or from isolated SVZ tissue also enriched PBX1 at the *THI* site, despite the fact that *TH* is not expressed in either cell population and H3K27^{me3} epigenetic marks prevail at the *THI* site in aNS (Fig. 8E-H, Fig. S7; (Cave et al., 2014)). We also compared by qPCR the transcript levels of *TH* and *DCX* in isolated SVZ, OB tissue and aNS cultures. *DCX*-expressing neuroblasts are present in the SVZ and OB, whereas *TH*-expressing PGNs are only found in the OB. Consistent with that, *TH*-expression in the SVZ and in aNS was barely detectable (Fig. 8I). Particularly in aNS, *DCX*-transcript levels, despite being overall very low, still exceeded those of *TH* by three orders of magnitude (Fig. F8I'). These findings reflect the bivalent configuration of the *DCX*-promoter/enhancer in aNS compared to the transcriptionally repressed state of the *TH*-gene promoter/enhancer in these cells. Moreover, our results are consistent with the notion that low levels of *DCX*-transcripts are already detectable in GFAP/prominin-double positive, bona-fide neural stem cells in the SVZ (Beckervordersandforth et al., 2010).

Discussion

Here, we describe sequential functions of *Pbx1* in the SVZ adult neural stem cell system. Using conditional ablation of *Pbx1* in adult neural progenitors or neuronally committed neuroblasts, together with ChIP-qPCR on the promoter/enhancers of selected downstream genes, we show that Pbx1 is required for the acquisition of a neuronal instead of oligodendroglial cell fate, necessary for the long-term survival of adult generated young neurons, and can bind its consensus sites in the regulatory regions of selected target genes well before these are transcriptionally activated.

Pbx1 is an intrinsic regulator of neurogenic versus oligodendrogliogenic cell fate decisions

Pbx1 is expressed in rapidly proliferating, ASCL1^{+}/Nestin^{+} progenitor cells in the SVZ. Its expression thus precedes that of MEIS2, which exhibits strong nuclear immunoreactivity only at the neuroblast stage and hence in a developmentally more restricted cell population of the SVZ (Agoston et al., 2014). Neural progenitor cells still possess the capacity to give rise to neurons, astrocytes and oligodendrocytes, whereas neuroblasts will mature exclusively into neurons. Notably when PBX1^{+} SVZ progenitor cells were differentiated *in vitro*, PBX1-immunoreactivity was retained in neurons and astrocytes but rapidly lost in oligodendrocytes. Neurogenesis and oligodendrogliogenesis are competing cell fates (Hack et al., 2004; Ortega et al., 2013). Specifically, by continuous live-imaging Ortega and colleagues found that the oligodendroglial lineage tree separates early from cells committed towards a neuro-astroglial fate. Given that targeted manipulation of MEIS2 with dominant-negative constructs in the SVZ caused a neurogenic to astrogliogenic fate switch (Agoston et al., 2014), our results argue that neuronal cell fate specification and differentiation in the adult SVZ involves the sequential activity of two TALE-HD proteins: PBX1 acts in an early progenitor cell population, directing it towards a neuronal as opposed to oligodendroglial fate, while MEIS2

is necessary for neuronal differentiation from more specified, neuro-astroglial progenitor cells. Our results may therefore have implications for the understanding of demyelinating pathologies: The number of SVZ-derived oligodendrocytes increases fourfold after a demyelinating lesion in the corpus callosum, indicating that stem- or early progenitor cells of the SVZ can respond to the insult by specifically upregulating the production of those cells that are needed for repair (Menn et al., 2006). According to the data presented above, this process should require downregulation of *Pbx1* as a direct response to the demyelinating stimulus.

PBX proteins cannot bind to DNA on their own (Longobardi et al., 2014; Penkov et al., 2013). Additional proteins thus need to participate in PBX1-dependent lineage decisions. Likely candidates are PAX6 or DLX2, which have known functions in SVZ neurogenesis and bind to TALE-HD proteins with high affinity in solution, or even additional proteins of the MEIS/PREP family (Agoston et al., 2014; Brill et al., 2008; Hack et al., 2005; Kohwi et al., 2005; 2008). However, no other member of this protein family, except MEIS2, has been implicated in SVZ neurogenesis so far. The precise composition of PBX1-containing transcriptional complexes in distinct cell population in the SVZ hence requires further investigation.

Pbx1 is required for the survival of adult generated neuroblasts

Genetic deletion of *Pax6* or forced expression of a function blocking form of MEIS2 in neuroblasts of the RMS elicits a cell fate change from dopaminergic to calretinin-expressing periglomerular interneurons (Agoston et al., 2014; Kohwi et al., 2005; Hack et al., 2005). Because both, PAX6 and MEIS2, form higher order protein complexes with PBX1, a decrease in the number of TH^{+} cells with a concomitant increase in calretinin^{+} cells was expected in dKO compared to sKO cells. However, instead of maturing towards an alternative PGN subtype fate, *Pbx1*/*Pbx2*-deficient neuroblasts were gradually eliminated from the OB, with

the first apoptotic dKO cells appearing in the rostral RMS. In addition, dKO cells were infrequently found in the GL and the majority of these exhibited ectopic upregulation of PBX3. Owing to the high structural homology of PBX proteins, PBX3 likely compensates for the loss of PBX1 and PBX2 during dopaminergic differentiation in dKO cells. Two scenarios may account for the predominant loss of dKO cells from the GL: dKO cells might be unable to reach the GL due to defective cell migration or they might be eliminated by cell death before they can reach the GL. The fact that we did not observe accumulating dKO cells in the RMS or anywhere during their radial migration in the GCL, together with the higher rate of programmed cell death in dKO compared to sKO cells, argues for compromised cell survival as an underlying cause. However, we cannot formally rule out any contributing migratory defect. It is worth pointing out that the high-affinity netrin receptor *deleted in colorectal cancer* (DCC) is downregulated in mesencephalic dopaminergic neurons in *Pbx1*-deficient animals (Sgado et al., 2012). However, we found no correlation between the localization of DCC and PBX1 in the OB, leaving an open question as to whether PBX1 also has a role in guiding neuroblasts during their migration in the OB (data not shown).

Interestingly, survival of dopaminergic PGNs requires the TALE-HD interacting transcription factor PAX6 (Ninkovic et al., 2010). Moreover, dopaminergic genes in *C. elegans*, including the worm homologue of the *TH*-gene, are cooperatively activated by the *Pbx* homologues *ceh-20, ceh-40* and *ceh-60*, together with *ceh-43*, a *Dlx* homologue (Doitsidou et al., 2013). Intriguingly, a *DLX* consensus binding site is present in close proximity to the *TH1* TALE-HD binding site, which is bound by PBX1 and MEIS2 (Agoston et al., 2014; Fig. 8). Together with the results presented above, these findings argue for a phylogenetically conserved role for PBX family proteins in dopaminergic neuron differentiation (Doitsidou et al., 2013).

PBX1 as pioneer factor in adult SVZ neurogenesis

We observed PBX1 binding to the regulatory regions of the downstream targets *DCX* and *TH* prior to their transcriptional activation. The presence of PBX1 at the *TH*-promoter/enhancer in chromatin isolated from the SVZ or aNS is particularly intriguing, as *TH*-transcript levels are not detectable and the *TH*-promoter carries repressive histone modifications in both cell populations, strongly suggesting that the *TH*-gene is transcriptionally silent in these cells. In fact, full maturation of dopaminergic OB neurons, including *TH*-expression, takes several weeks and requires odor-mediated afferent synaptic activity (Akiba et al., 2009; Baker and Farbman, 1993; Baker et al., 1988; Winner et al., 2002). Moreover, aNS in culture will not express *TH*, even with specialized differentiation protocols, unless they are genetically modified (Cave et al., 2014; Deleidi et al., 2011). PBX1 chromatin binding can thus anticipate *de novo* transcriptional activation of the *TH*-gene by weeks if not months, suggestive of a pioneer-function for PBX1 in this context. Pioneer factors are a special class of transcriptional regulators that can penetrate silent chromatin and bind regulatory regions at times when the overall chromatin structure still prevents access of other transcription factors (Iwafuchi-Doi and Zaret, 2014). Notably, observations made in the context of skeletal muscle development, hindbrain patterning, or breast cancer had already indicated a role for PBX1 in transcriptional priming in these systems (Choe et al., 2014; Berkes et al., 2004; Magnani et al., 2011). Specifically during skeletal muscle differentiation, PBX1 is constitutively bound to the promoter of the *Myogenin* (MyoG) gene and transcriptional activation of this promoter requires recruitment of the pro-myogenic transcription factor MYOD by PBX1 (Berkes et al., 2004). Likewise, PBX4 primes the *hoxb1a* promoter during zebrafish hindbrain development, whereas in the breast cancer cell line MCF7, PBX1 acts as pioneer factor for the estrogen receptor alpha (ERα)- dependent transcriptional program following estrogen stimulation (Magnani et al., 2011). Thus in addition to its role in the regulation of neurogenic cell fate decisions and the survival of newly generated neurons, our results suggest that PBX1 may act

as initial 'mark' that endows the *DCX-* and *TH*-genes with the competence for later activation in the SVZ adult neurogenic system. Collectively, the present study establishes a role for PBX1 in adult SVZ neurogenesis that goes beyond that of its heterodimerization partner MEIS2.

MATERIALS AND METHODS

Animals and stereotactic injections

Stereotactic injections in 8- to 12-week-old $Pbx1^{fl/fl}$;$Pbx2^{-/-}$ mice of mixed gender (Koss et al., 2012; Selleri et al., 2004) were performed as described and with published coordinates (Brill et al., 2008; Agoston et al., 2014; Hack et al., 2005). Animals received independent injections into both hemispheres. The number of animals examined per experimental setting are given in Table S4. All procedures involving animals were approved by the local animal care committee and are in accordance with the law for animal experiments issued by the state government. Statistical analysis was performed with two-tailed, unpaired Student's t-test (Prism 5.01, Graph Pad); the s.e.m. represents variance between different injections. For the lineage tracing with tdTomato- and Cre-GFP-expressing viruses, a mixture of both viral stocks, diluted to equal titers, was injected into $Pbx1^{fl/fl}$;$Pbx2^{-/-}$ littermates. In each series of experiments, all animals received injections from the same pre-mixed viral stock. For analysis, serial, 75µm thick vibratome sections of the OB were cut and every third section was stained with antibodies specific for tdTomato or GFP. Fig. 6F shows the absolute number of cells that could be recovered from for each genotype by this approach.

In situ hybridization and immunohistochemical analyses

In situ hybridization was performed on 75µm thick vibratome section as described (Heine et al., 2008). The *Pbx1*-specific probe comprised NT 1510 to 2398 of NCBI AF202197, the *Pbx2*-specific probe NT 1045 to 1916 of NCBI NM_017463. For immunocytochemical and immunohistochemical staining, cells were fixed with 2% paraformaldehyde (PFA) in phosphate buffered saline pH 7.4 (PBS). Free-floating aNS were allowed to attach to poly-D-lysine coated coverslips for 30min prior to fixation. Immunohistochemical analysis on PFA-perfused frozen or vibratome brain sections was performed as described (Agoston et al.,

2014). Primary and secondary antibodies are listed in Table S1. Images were taken with a Nikon 80i or a Nikon Eclipse TE2000-E confocal microscope. The number of specimens and sample sizes analyzed are given in Table S3. Cells were counted blind. Standard deviation was calculated between technical replicates with unpaired student's t-test. Chromogen staining was performed with a VENTANA DISCOVERY XT automated staining system, with antigen retrieval protocol Conditioner #1, Omni-Map HRP detection and counterstaining with hematoxylin.

Chromatin immunoprecipitation (ChIP)

ChIP-analysis from tissues or cells was performed as described (Agoston et al., 2014). Antibodies and primers used for ChIP are specified in Table S2. Experiments were conducted at least in triplicates and plotted as s.e.m.. Statistical analysis was performed with two-tailed, unpaired Student's t-test between experimental samples and the control sample precipitated with normal IgG antibodies.

Cell culture

Sphere forming cells were isolated from the lateral walls of the lateral ventricle of 8 - 12 week old C57BL/6 mice and propagated under non-adherent conditions as described (Agoston et al., 2014). Unless otherwise noted, passage 1 aNS, cultured for no more than 5 days were used for infection with GFP- or Cre-GFP-expressing viruses. For quantification, experiments were counted blind; statistical analysis was performed with two-tailed, paired Student's t-test between GFP- or Cre-GFP-transduced cell cohorts. To obtain cultures enriched for neurons for ChIP, aNS were transduced with *Pax6* followed by differentiation on laminin-coated dishes ($1\mu g/cm^2$) in medium containing 2ng/ml bFGF and 20ng/ml brain-derived neurotrophic factor (BDNF). To obtain cultures enriched for astrocytes, aNS were differentiated on poly-D-

lysine coated dishes (140µg/ml) in medium containing 10ng/ml ciliary neurotrophic factor (CNTF) and 0.5% FCS.

For the label-retaining assay, primary aNS were grown for 24 hours and then pulsed for one hour with 2.5µM 5-Carboxyfluorescein Diacetate, acetoxymethyl ester (C1354, Thermo Fisher Scientific) for 5 minutes at room temperature, washed and cultured at 37°C. After four days, the spheres were dissociated and grown for 24 hours on laminin-coated dishes in the presence of EGF and bFGF prior to immunohistochemical analysis. Because under these conditions occasionally cells spontaneously exit the cell cycle and differentiate, cultures were stained for the stem-/progenitor cell marker Nestin. Only Nestin$^+$/CFDA$^+$ cells were counted as quiescent neural stem cells *in vitro*. The number of technical replicates and number of cells counted for each experiment is given in Table S4.

Retroviral transduction and reporter assay

Retroviral constructs were pCLIG-GFP, or corresponding vectors carrying a Cre-IRES-GFP cassette or tdTomato (Brill et al., 2008; Hildinger et al., 1999; Hojo et al., 2000). Virus production was performed as detailed (Agoston et al., 2014). Viral titers were between 4.7×10^6 and 1.7×10^7 p.f.u.. Viral stocks of were diluted to equal titers before use. Reporter assays with a luciferase reporter under control of the 2073bp endogenous promoter/enhancer of the *DCX*-gene (Piens et al., 2010) cloned in pGL3-basic and the Pbx1a-pCS2$^+$ and Pbx1b-pCS2$^+$ mammalian expression plasmids were performed as described (Agoston et al., 2014). For deletion of the *DCXI* site, site-directed mutagenesis was carried out with the primers 5-gtgattaaaatcatgcatatatcttgcatt and 5-tgaaaatagaaacagcccagatgtctgt on a *DCX* promoter/enhancer comprising NT 1-1870 of Piens et al. (2010) (Phusion Site-Directed Mutagenesis Kit, New England Bioloabs). Transcription factor binding site prediction was performed with the MatInspector (Genomatix Software Suite; Cartharius et al., 2005). siRNA-mediated knockdown of *Pbx1* was carried out with Silencer® Select siRNAs (5`-

guuggaccaacgugcaau-3; 50pmol transfected per $2x10^6$ cells; Life Technologies). Non-targeting control siRNAs were purchased from Eurogentech (SR-CL000-005). RNA duplexes were transfected with Metafectene Pro (Biontex). After siRNA transfection, cells were grown for 48 hours as free-floating spheres before they were used for ChIP.
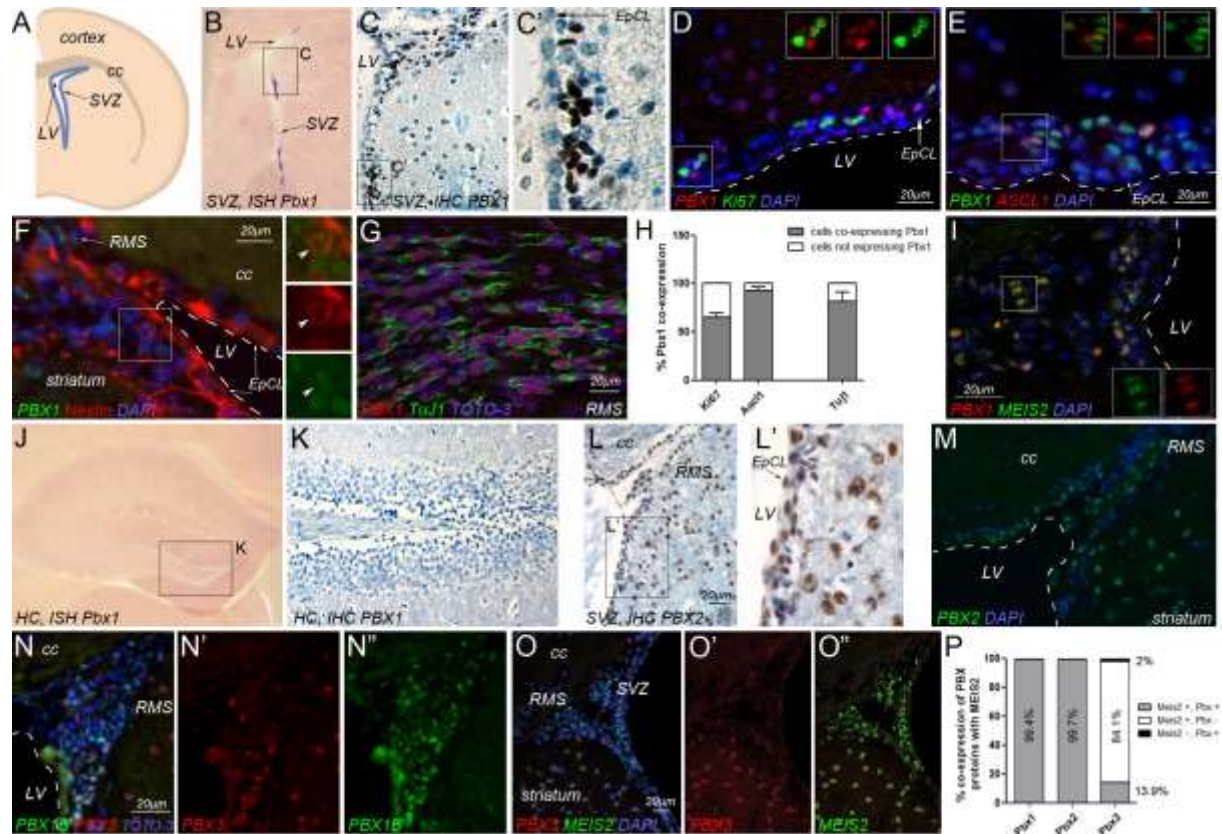
Figures

Fig. 1. *Pbx*-expression in the SVZ. (A) Schematic representation of the adult mouse SVZ. (B) *In situ* hybridization for *Pbx1* transcripts (blue) in the SVZ. (C) PBX1 protein (brown) in the SVZ, cell nuclei are counterstained in blue; the boxed area is shown at higher magnification in (C'). (D-F) Immunofluorescence double-labeling for PBX1 (red) and Ki67 (green, D; n=4 hemispheres), PBX1 (green) and ASCL1 (red, E; n=2 hemispheres), PBX1 (green) and Nestin (red, F; n=2 hemispheres); boxed areas are shown as single channels. The arrow in (D) marks the EpCL, the arrowhead in (F) a representative Nestin+/PBX1+ cell located adjacent to the EpCL. (G) PBX1 (red) protein in migrating, TuJ1+ neuroblasts (green) in the RMS. (H) Quantification of co-localization; error bars indicate s.e.m.. (I) PBX1 (red) and MEIS2 (green) in neuroblasts at the beginning of the RMS (n=4 hemispheres). (J, K)

Lack of Pbx1 transcript (J) and protein (K) in the hippocampus. (L-M) PBX2 protein in the SVZ and RMS; ependymal and striatal cells are strongly, cells in the subependyma are weakly immunoreactive for PBX2. (N, O) Double-stainings reveal limited overlap between PBX3 (red) and PBX1B (green, N; n=2 hemispheres) or MEIS2 (green, O; n=4 hemispheres) in the SVZ. The PBX1B antibody was used for double IFC with PBX3 or MEIS2 (both rabbit polyclonal antibodies); PBX1B is the prominent PBX1 isoform expressed in SVZ-derived stem-/progenitor cells (Fig. S6). (P) Quantification of co-localization of MEIS2 with different PBX family proteins in the SVZ and emerging RMS. [cc: corpus callosum; EpCL: ependymal cell layer; HC: hippocampus; IHC: immunhistochemistry; ISH: *in situ* hybridization; LV: lateral ventricle; RMS: rostral migratory stream; SVZ: subventricular zone].
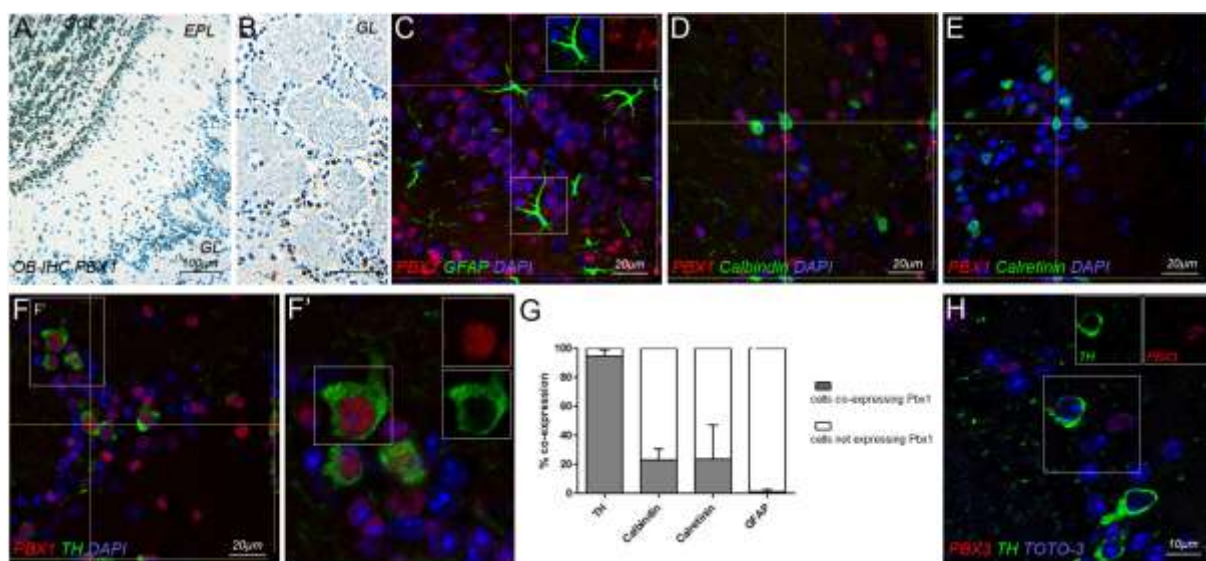
Fig. 2. PBX localization in the OB. (A, B) PBX1 protein (brown) in the GCL and GL of the OB. (C-F) Double-labeling for PBX1 (red) and GFAP (green) in the GCL (C), and calbindin (green, D), calretinin (green, E), and TH (green, F) in the GL; boxed areas are shown as single channels or higher magnification respectively. (G) Quantification of the results; error bars indicate s.e.m. (n=4 hemispheres each). (H) PBX3 (red) was not detected in TH^{+} cells (green). [EPL: external plexiform layer; GCL: granule cell layer; GL: glomerular layer; TH: tyrosin hydroxylase].
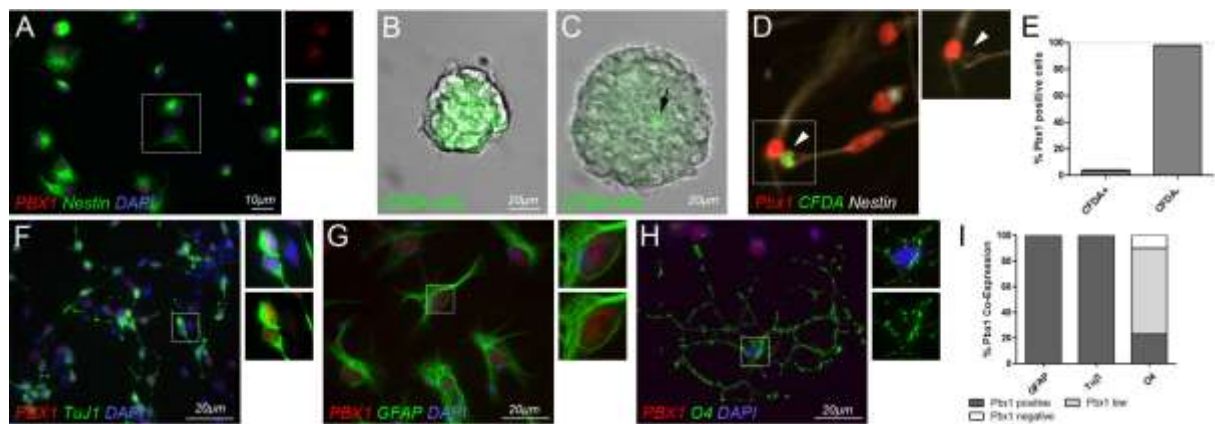
Fig. 3. PBX1 localization in aNS cultures *in vitro*. (A) PBX1 protein in Nestin[+], SVZ-derived aNS cells. (B-D) CFDA-label retaining, bona-fide stem cells in aNS are PBX1-negative; (B) primary aNS 4 hours after incubation with CFDA AM; (C) primary aNS after two days in culture; the arrow in (C) marks a single label-retaining cell; (D) stem-/progenitor cells 4 days after CFDA labeling, dissociated and grown for 24 hours as adherent culture on laminin in the presence of EGF/bFGF; representative example of a label-retaining (green), Nestin[+] cell (white), which is immunonegative for PBX1 (red). (E) Quantification of the results. (F-H) PBX1 (red) in *in vitro* differentiated neurons (TuJ1, green, F), astroglia (GFAP, green, G) or oligodendrocytes (O4, green, H). (I) Proportional of PBX1-immunoreactive neurons, astroglia and oligodendrocytes after 3d of *in vitro* differentiation. 'Pbx1 low': weak immunoreactivity, possibly reflecting ongoing PBX1 downregulation in oligodendrocytes. All experiments were performed in three biological replicates (Table S3).
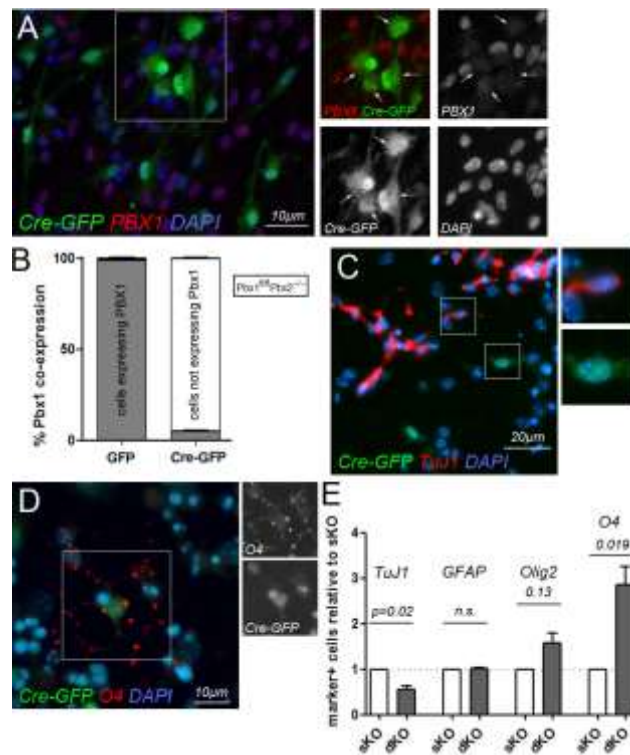
Fig. 4. *Pbx1* **loss-of-function alters neuro-oligodendroglial fate decisions** *in vitro* (A) *Pbx1*fl/fl;*Pbx2*-/- aNS cultures infected with Cre-GFP expressing retroviruses to generate dKO cells stained for PBX1 (red); the boxed area is shown as single channels, arrows mark Cre-GFP transduced cells. (B) Quantification of PBX1 localization in GFP and Cre-GFP transduced cells (n=2 each). (C, D) Immunofluorescence detection of TuJ1+ neurons (C; n=3)) or O4+ oligodendroglia (D; n=4)) in Cre-GFP transduced *Pbx1*fl/fl;*Pbx2*-/- aNS cultures. Boxed areas are shown in single channels in (A, C, D). (E) Quantification of the results; error bars indicate s.e.m..
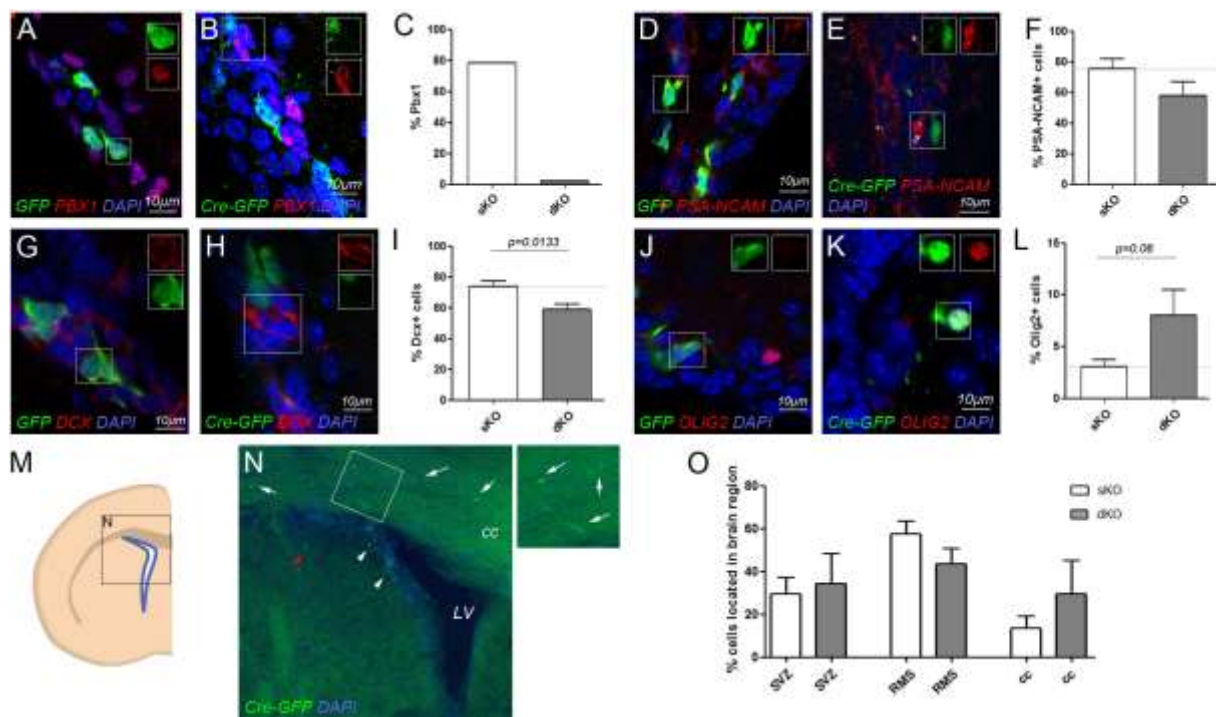
Fig. 5. *Pbx1* **loss-of-function in SVZ stem- and progenitor cells alters neuro-oligodendroglial fate decisions** *in vivo***.** (A-C) Neuroblasts migrating in the RMS of *Pbx1*^{fl/fl};*Pbx2*^{-/-} animals transduced with GFP stain for PBX1 (red, A, C; n=1 animal, 2 hemispheres) while cells transduced with Cre-GFP do not (B, C; n=1 animal, 2 hemispheres). (D-K) GFP- (D, G, J) and Cre-GFP- (E, H, K) transduced cells in the SVZ stained for the markers indicated: (D-F) PSA-NCAM (n=5 animals for GFP, n=4 animals for Cre-GFP), (G-I) DCX (n=5 animals for GFP, n=6 animals for Cre-GFP), (J-L) OLIG2 (n=7 animals for GFP, n=7 animals for Cre-GFP. (F, I, L) Quantification of the results. (M) Schematic drawing of the brain region shown in (N). (N) 3 days after virus injection into the SVZ, some Cre-GFP-transduced cells populate the SVZ (white arrowheads), while others migrated into the cc (arrows) or striatum (red arrowhead). (O) Quantification of GFP- or Cre-GFP transduced cells found in the SVZ, RMS (integrated into the chain of migrating cells) or cc (corpus callosum), 3 days after virus injection into the SVZ. Error bars indicate s.e.m. (n=7 animals each).
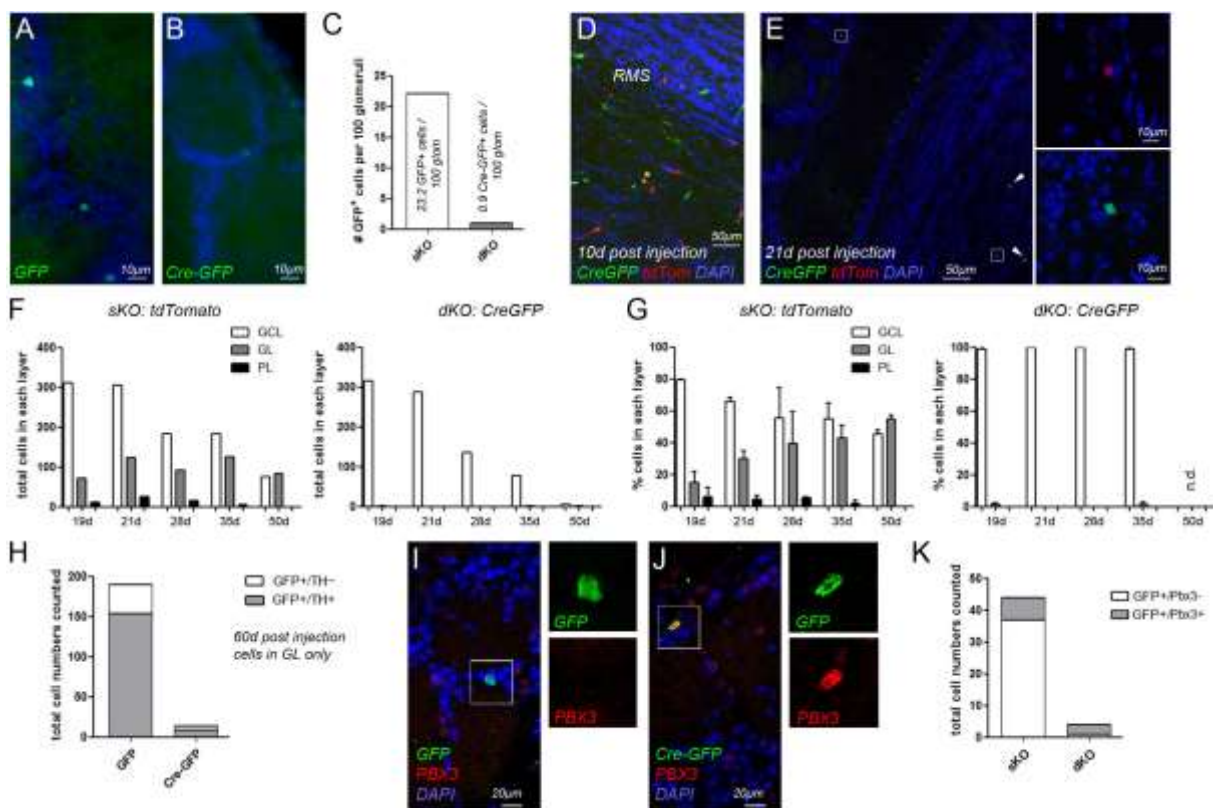
Fig. 6. Targeted *Pbx1*-deletion in migrating neuroblasts compromises cell survival. (A-C) sKO (A) but not dKO cells (B) are present in the GL 60 days after GFP- or Cre-GFP transduction of migrating neuroblasts in the RMS of *Pbx1*^{fl/fl};*Pbx2*^{-/-} animals (n=4 animals for GFP, n=5 animals for Cre). (D) Quantification of the results. (D-G) Tracing sKO (tdTomato-transduced, red) and dKO (Cre-GFP-transduced, green) cells in the OB at different times after simultaneous injection of both retroviruses into the RMS of *Pbx1*^{fl/fl};*Pbx2*^{-/-} animals. (D) Cross section of the inner OB 10 days post injection; sKO and dKO cells migrate into the GCL; the asterisk marks one of very few double-infected cells observed. (E) Cross-section of the outer OB 21 days post injection; sKO cells have entered the GL, dKO cells are found in the GCL (arrowheads). (F) Absolute numbers of sKO and dKO cells found in the GCL, PGL and GL at different times after virus injection; n=2 animals, 4 hemispheres per condition;

cells were counted in every third section of the OB, total cell counts are displayed. Although cell numbers decline in both cohorts, sKO cell migrate from the GCL through the PL to settle in the GL, whereas few dKO cells appear in the GL even at late times post viral transduction. (G) Relative proportion of sKO and dKO cells found in each OB layer at the times analyzed; because of the very low number of dKO that survived at 50 days post infection, no relative distribution was calculated; error bars indicate s.e.m.. (H) Proportion of TH$^+$ cells among GFP-transduced (sKO) and Cre-GFP-transduced (dKO) cells 60 days after separate injection of GFP- or Cre-GFP-expressing viruses into the RMS of *Pbx1*$^{fl/fl}$;*Pbx2*$^{-/-}$ animals (n=2 animals, 4 hemispheres for GFP, n=3 animals, 6 hemispheres for TH). (I, J) Representative images of sKO (I) and dKO (J) cells stained for PBX3 (n=1 animal, 2 hemispheres for GFP, Cre-GFP each). Boxed areas are shown at higher magnification in separate panels in (E, I, J). (K) Quantification of the results. [n.d.: not determined; PL: internal/external plexiform layer].
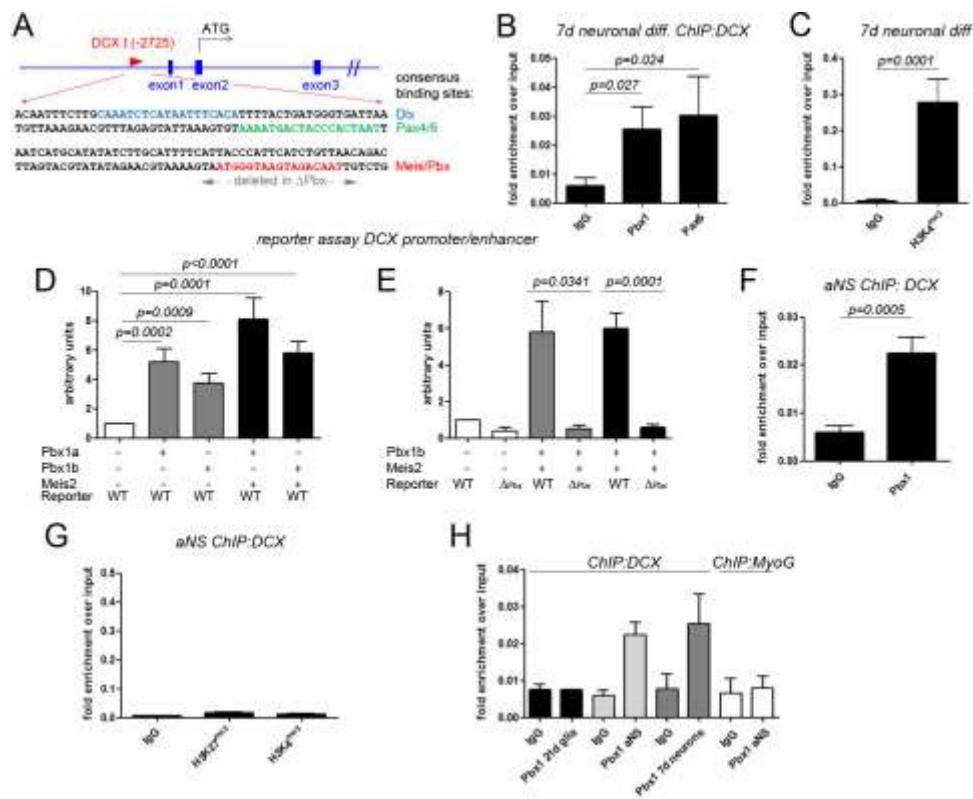
Fig. 7. PBX1 binds the *DCX*-promoter/enhancer prior to its activation. (A) Schematic representation of the *DCX*-promoter/enhancer, the sequence of the 100bp *DCXI* ChIP amplicon is given below; consensus binding sites for DLX, PAX4/PAX6 and PBX/MEIS are highlighted. (B, C) ChIP-qPCR results for the *DCXI*-site on chromatin of *in vitro* differentiated neurons with the antibodies indicated; n=4. (D) Activation of a *DCX*-driven luciferase reporter (Piens et al., 2010) by splice isoforms PBX1a and PBX1b, with or without MEIS2, in HEK293T cells; n=5. (E) Reporter activity of a 1870bp *DCX* promoter/enhancer construct with (ΔPBX) or without (WT) deletion of the MEIS/PBX consensus site; n=5. (F) ChIP for PBX1 at *DCXI* in aNS; n=4. (G) The *DCXI*-site in aNS lacks activating and repressive histone marks; n=4. (H) The PBX1-antibody does not enrich the *DCXI* site in *in vitro* differentiated astroglia or a known PBX1-target site in the promoter of *MyoG* (Berkes et al., 2004) in aNS; n=3.
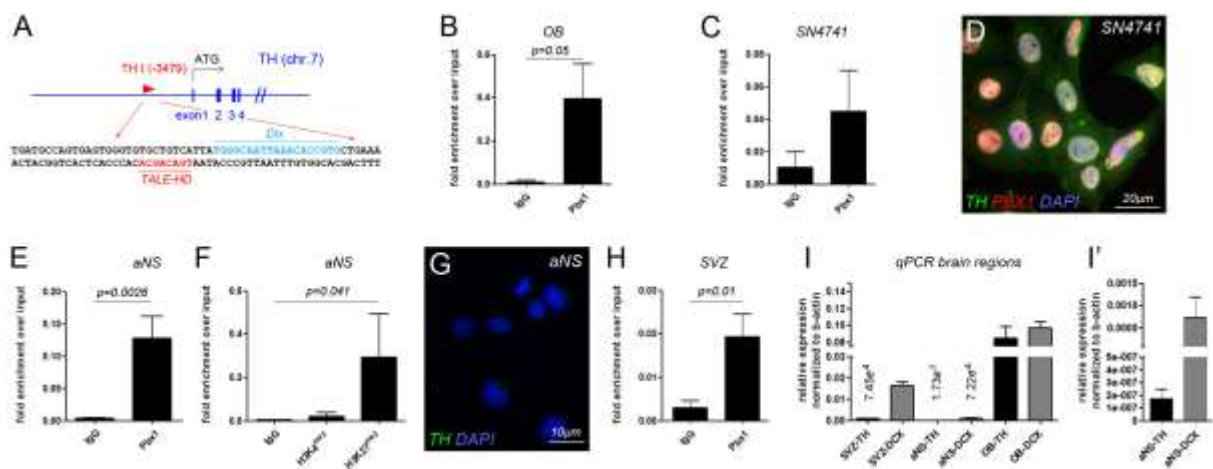
Fig. 8. PBX1 binds the *TH*-promoter/enhancer already at the progenitor cell state. (A) Schematic representation of the *TH*-promoter/enhancer; the sequence of the 70bp *THI* ChIP amplicon is given below; consensus binding sites for DLX and PBX/MEIS are highlighted. (B, C) PBX1 binding to *THI* by ChIP-qPCR in mouse adult OB (B; n=4) and SN4741 cells (C; n=3). (D) TH immunoreactivity in SN4741 cells. (E-F) ChIP-qPCR results for PBX1 (E; n=3) and histone modifications (F; n=3) on *THI* in aNS. (G) Lack of *TH*-expression in aNS. (H) PBX1 binding to *THI* in the SVZ (n=5). (I) Transcript expression of *TH* in comparison to *DCX* in different brain regions as determined by qPCR (SVZ: n=3, aNS:n=4, OB:n=4). (I') Comparison of *TH*- and *DCX*-transcript levels in aNS at higher resolution; Consistent with the lack of repressive histone modifications at the *DCX*-promoter/enhancer, transcription off this promoter, despite being overall low, exceeds that of *TH* by three orders of magnitude. Error bars indicate s.e.m.

References

Agoston, Z., Heine, P., Brill, M. S., Grebbin, B. M., Hau, A.-C., Kallenborn-Gerhardt, W., Schramm, J., Götz, M. and Schulte, D. (2014). Meis2 is a Pax6 co-factor in neurogenesis and dopaminergic periglomerular fate specification in the adult olfactory bulb. *Development* **141**, 28–38.

Akiba, Y., Sasaki, H., Huerta, P. T., Estevez, A. G., Baker, H. and Cave, J. W. (2009). gamma-Aminobutyric acid-mediated regulation of the activity-dependent olfactory bulb dopaminergic phenotype. *J. Neurosci. Res.* **87**, 2211–21.

Baker, H. and Farbman, A. I. (1993). Olfactory afferent regulation of the dopamine phenotype in the fetal rat olfactory system. *Neuroscience* **52**, 115–134.

Baker, H., Towle, A. C. and Margolis, F. L. (1988). Differential afferent regulation of dopaminergic and GABAergic neurons in the mouse main olfactory bulb. *Brain Res.* **450**, 69–80.

Barami, K., Sloan, A. E., Rojiani, A., Schell, M. J., Staller, A. and Brem, S. (2009). Relationship of gliomas to the ventricular walls. *J. Clin. Neurosci.* **16**, 195–201.

Barski, A., Cuddapah, S., Cui, K., Roh, T. Y., Schones, D. E., Wang, Z., Wei, G., Chepelev, I. and Zhao, K. (2007). High-Resolution Profiling of Histone Methylations in the Human Genome. *Cell* **129**, 823–837.

Beckervordersandforth, R., Tripathi, P., Ninkovic, J., Bayam, E., Lepier, A., Stempfhuber, B., Kirchhoff, F., Hirrlinger, J., Haslinger, A., Lie, D. C., et al. (2010). In vivo fate mapping and expression analysis reveals molecular hallmarks of prospectively isolated adult neural stem cells. *Cell Stem Cell* **7**, 744–58.

Berkes, C. a, Bergstrom, D. a, Penn, B. H., Seaver, K. J., Knoepfler, P. S. and Tapscott, S. J. (2004). Pbx marks genes for activation by MyoD indicating a role for a homeodomain protein in establishing myogenic potential. *Mol. Cell* **14**, 465–77.

Biebl, M., Cooper, C. M., Winkler, J. and Kuhn, H. G. (2000). Analysis of neurogenesis and programmed cell death reveals a self-renewing capacity in the adult rat brain. *Neurosci. Lett.* **291**, 17–20.

Brendolan, A., Ferretti, E., Salsi, V., Moses, K., Quaggin, S., Blasi, F., Cleary, M. L. and Selleri, L. (2005). A Pbx1-dependent genetic and transcriptional network regulates spleen ontogeny. *Development* **132**, 3113–26.

Brill, M. S., Snapyan, M., Wohlfrom, H., Ninkovic, J., Jawerka, M., Mastick, G. S., Ashery-Padan, R., Saghatelyan, A., Berninger, B. and Götz, M. (2008). A dlx2- and pax6-dependent transcriptional code for periglomerular neuron specification in the adult olfactory bulb. *J. Neurosci.* **28**, 6439–52.

Capellini, T. D., Zappavigna, V. and Selleri, L. (2011). Pbx homeodomain proteins: TALEnted regulators of limb patterning and outgrowth. *Dev. Dyn.* **240**, 1063–86.

Cartharius, K., Frech, K., Grote, K., Klocke, B., Haltmeier, M., Klingenhoff, A., Frisch, M., Bayerlein, M., and Werner, T. (2005). MatInspector and beyond: promoter analysis based on transcription factor binding sites. *Bioinformatics* **21**, 2933-42.

Cattaneo, E. and McKay, R. (1990). Proliferation and differentiation of neuronal stem cells regulated by nerve growth factor. *Nature* **347**, 762–5.

Cave, J. W., Wang, M. and Baker, H. (2014). Adult subventricular zone neural stem cells as a potential source of dopaminergic replacement neurons. *Front. Neurosci.* **8**, 16.

Choe, S.K., Ladam, F. and Sagerström, C.G. (2014). TALE factors poise promoters for activation by HOX proteins. *Dev. Cell* **28**, 203-11

Deleidi, M., Cooper, O., Hargus, G., Levy, A. and Isacson, O. (2011). Oct4-induced reprogramming is required for adult brain neural stem cell differentiation into midbrain dopaminergic neurons. *PLoS One* **6**,.

DiMartino, J. F., Selleri, L., Traver, D., Firpo, M. T., Rhee, J., Warnke, R., O'Gorman, S., Weissman, I. L. and Cleary, M. L. (2001). The Hox cofactor and proto-oncogene Pbx1 is required for maintenance of definitive hematopoiesis in the fetal liver. *Blood* **98**, 618–26.

Doetsch, F., Petreanu, L., Caille, I., Garcia-Verdugo, J. M. and Alvarez-Buylla, A. (2002). EGF converts transit-amplifying neurogenic precursors in the adult brain into multipotent stem cells. *Neuron* **36**, 1021–1034.

Doitsidou, M., Flames, N., Topalidou, I., Abe, N., Felton, T., Remesal, L., Popovitchenko, T., Mann, R., Chalfie, M. and Hobert, O. (2013). A combinatorial regulatory signature controls terminal differentiation of the dopaminergic nervous system in C. elegans. *Genes Dev.* **27**, 1391–405.

Ferretti, E., Li, B., Zewdu, R., Wells, V., Hebert, J. M., Karner, C., Anderson, M. J., Williams, T., Dixon, J., Dixon, M. J., et al. (2011). A conserved Pbx-Wnt-p63-Irf6 regulatory module controls face morphogenesis by promoting epithelial apoptosis. *Dev. Cell* **21**, 627–41.

Golonzhka, O., Nord, A., Tang, P.L., Lindtner, S., Ypsilanti, A.R., Ferretti, E., Visel, A., Selleri, L. and Rubenstein, J.L. (2015). Pbx regulates patterning of the cerebral cortex in progenitors and postmitotic neurons. *Neuron* **88**, 1192-207

Gordon, J. a R., Hassan, M. Q., Koss, M., Montecino, M., Selleri, L., van Wijnen, A. J., Stein, J. L., Stein, G. S. and Lian, J. B. (2011). Epigenetic regulation of early osteogenesis and mineralized tissue formation by a HOXA10-PBX1-associated complex. *Cells. Tissues. Organs* **194**, 146–50.

Hack, M. A, Saghatelyan, A., de Chevigny, A., Pfeifer, A., Ashery-Padan, R., Lledo, P.M. and Götz, M. (2005). Neuronal fate determinants of adult olfactory bulb neurogenesis. *Nat. Neurosci.* **8**, 865–72.

Heine, P., Dohle, E., Bumsted-O'Brien, K., Engelkamp, D. and Schulte, D. (2008). Evidence for an evolutionary conserved role of homothorax/Meis1/2 during vertebrate retina development. *Development* **135**, 805–11.

Hildinger, M., Abel, K.L., Ostertag, W., Baum, C. (1999). Design of 5' untranslated sequences in retroviral vectors for medical use. *J. Virol.* **73**, 4083-9.

Hojo, M., Ohtsuka, T., Hashimoto, N., Gradwohl, G., Guillemot, F. and Kageyama, R. (2000). Glial cell fate specification modulated by the bHLH gene Hes5 in mouse retina. *Development* **127**, 2515–2522.

Iwafuchi-Doi, M. and Zaret, K. S. (2014). Pioneer transcription factors in cell reprogramming. *Genes Dev.* **28**, 2679–2692.

Karl, C., Couillard-Despres, S., Prang, P., Munding, M., Kilb, W., Brigadski, T., Plötz, S., Mages, W., Luhmann, H., Winkler, J., et al. (2005). Neuronal precursor-specific activity of a human doublecortin regulatory sequence. *J. Neurochem.* **92**, 264–82.

Kim, E. J., Leung, C. T., Reed, R. R. and Johnson, J. E. (2007). In vivo analysis of Ascl1 defined progenitors reveals distinct developmental dynamics during adult neurogenesis and gliogenesis. *J. Neurosci.* **27**, 12764–74.

Kohwi, M., Osumi, N., Rubenstein, J. L. R. and Alvarez-Buylla, A. (2005). Pax6 is required for making specific subpopulations of granule and periglomerular neurons in the olfactory bulb. *J. Neurosci.* **25**, 6997–7003.

Kohwi, M., Petryniak, M. A., Long, J. E., Ekker, M., Obata, K., Yanagawa, Y., Rubenstein, J. L. R. and Alvarez-Buylla, A. (2007). A subpopulation of olfactory bulb GABAergic interneurons is derived from Emx1- and Dlx5/6-expressing progenitors. *J. Neurosci.* **27**, 6878–6891.

Koss, M., Bolze, A., Brendolan, A., Saggese, M., Capellini, T. D., Bojilova, E., Boisson, B., Prall, O. W. J., Elliott, D. a, Solloway, M., et al. (2012). Congenital asplenia in mice and humans with mutations in a Pbx/Nkx2-5/p15 module. *Dev. Cell* **22**, 913–26.

Ladam, F. and Sagerström, C. G. (2014). Hox regulation of transcription: More complex(es). *Dev. Dyn.* **243**, 4–15.

Lendahl, U., Zimmerman, L. B. and McKay, R. D. (1990). CNS stem cells express a new class of intermediate filament protein. *Cell* **60**, 585–95.

Lim, D. a and Alvarez-Buylla, A. (2014). Adult neural stem cells stake their ground. *Trends Neurosci.* **37**, 563–571.

Longobardi, E., Penkov, D., Mateos, D., De Florian, G., Torres, M. and Blasi, F. (2014). Biochemistry of the tale transcription factors PREP, MEIS, and PBX in vertebrates. *Dev. Dyn.* **243**, 59–75.

Magnani, L., Ballantyne, E. B., Zhang, X. and Lupien, M. (2011). PBX1 genomic pioneer function drives ERα signaling underlying progression in breast cancer. *PLoS Genet.* **7**, e1002368.

Manley, N. R., Selleri, L., Brendolan, A., Gordon, J. and Cleary, M. L. (2004). Abnormalities of caudal pharyngeal pouch development in Pbx1 knockout mice mimic loss of Hox3 paralogs. *Dev. Biol.* **276**, 301–12.

Menn, B., Garcia-Verdugo, J. M., Yaschine, C., Gonzalez-Perez, O., Rowitch, D. and Alvarez-Buylla, A. (2006). Origin of oligodendrocytes in the subventricular zone of the adult brain. *J. Neurosci.* **26**, 7907–18.

Ninkovic, J., Pinto, L., Petricca, S., Lepier, A., Sun, J., Rieger, M. A., Schroeder, T., Cvekl, A., Favor, J. and Götz, M. (2010). The transcription factor Pax6 regulates survival of dopaminergic olfactory bulb neurons via crystallin αA. *Neuron* **68**, 682–694.

Ortega, F., Gascón, S., Masserdotti, G., Deshpande, A., Simon, C., Fischer, J., Dimou, L., Chichung Lie, D., Schroeder, T. and Berninger, B. (2013). Oligodendrogliogenic and neurogenic adult subependymal zone neural stem cells constitute distinct lineages and exhibit differential responsiveness to Wnt signalling. *Nat. Cell Biol.* **15**, 602–13.

Pastrana, E., Cheng, L.-C. and Doetsch, F. (2009). Simultaneous prospective purification of adult subventricular zone neural stem cells and their progeny. *Proc. Natl. Acad. Sci. U. S. A.* **106**, 6387–92.

Pastrana, E., Silva-Vargas, V. and Doetsch, F. (2011). Eyes wide open: a critical review of sphere-formation as an assay for stem cells. *Cell Stem Cell* **8**, 486–98.

Penkov, D., Mateos San Martín, D., Fernandez-Díaz, L. C., Rosselló, C. a, Torroja, C., Sánchez-Cabo, F., Warnatz, H. J., Sultan, M., Yaspo, M. L., Gabrieli, A., et al. (2013). Analysis of the DNA-binding profile and function of TALE homeoproteins reveals their specialization and specific interactions with Hox genes/proteins. *Cell Rep.* **3**, 1321–33.

Petreanu, L. and Alvarez-Buylla, A. (2002). Maturation and death of adult-born olfactory bulb granule neurons: role of olfaction. *J. Neurosci.* **22**, 6106–13.

Piens, M., Muller, M., Bodson, M., Baudouin, G. and Plumier, J.-C. (2010). A short upstream promoter region mediates transcriptional regulation of the mouse doublecortin gene in differentiating neurons. *BMC Neurosci.* **11**, 64.

Redmond, L., Hockfield, S. and Morabito, M. a (1996). The divergent homeobox gene PBX1 is expressed in the postnatal subventricular zone and interneurons of the olfactory bulb. *J. Neurosci.* **16**, 2972–82.

Reynolds, B. A. and Rietze, R. L. (2005). Neural stem cells and neurospheres--re-evaluating the relationship. *Nat. Methods* **2**, 333–6.

Reynolds, B. A. and Weiss, S. (1992). Generation of neurons and astrocytes from isolated cells of the adult mammalian central nervous system. *Science* **255**, 1707–10.

Reynolds, B. A. and Weiss, S. (1996). Clonal and population analyses demonstrate that an EGF-responsive mammalian embryonic CNS precursor is a stem cell. *Dev. Biol.* **175**, 1–13.

Sakamoto, M., Ieki, N., Miyoshi, G., Mochimaru, D., Miyachi, H., Imura, T., Yamaguchi, M., Fishell, G., Mori, K., Kageyama, R., et al. (2014). Continuous postnatal neurogenesis contributes to formation of the olfactory bulb neural circuits and flexible olfactory associative learning. *J. Neurosci.* **34**, 5788–99.

Schulte, D. (2014). Meis: New friends of Pax, *Neurogenesis*, **1:1**, e976014

Selleri, L., Depew, M. J., Jacobs, Y., Chanda, S. K., Tsang, K. Y., Cheah, K. S., Rubenstein, J. L., O'Gorman, S. and Cleary, M. L. (2001). Requirement for Pbx1 in skeletal patterning and programming chondrocyte proliferation and differentiation. *Development* **128**, 3543–57.

Selleri, L., DiMartino, J., van Deursen, J., Brendolan, A., Sanyal, M., Boon, E., Capellini, T., Smith, K. S., Rhee, J., Pöpperl, H., et al. (2004). The TALE homeodomain protein Pbx2 is not essential for development and long-term survival. *Mol. Cell. Biol.* **24**, 5324–5331.

Sgadò, P., Ferretti, E., Grbec, D., Bozzi, Y. and Simon, H. H. (2012). The atypical homeoprotein Pbx1a participates in the axonal pathfinding of mesencephalic dopaminergic neurons. *Neural Dev.* **7**, 24.

Son, J. H., Chun, H. S., Joh, T. H., Cho, S., Conti, B. and Lee, J. W. (1999). Neuroprotection and neuronal differentiation studies using substantia nigra dopaminergic cells derived from transgenic mouse embryos. *J. Neurosci.* **19**, 10–20.

Stankunas, K., Shang, C., Twu, K. Y., Kao, S.-C., Jenkins, N. a, Copeland, N. G., Sanyal, M., Selleri, L., Cleary, M. L. and Chang, C.-P. (2008). Pbx/Meis deficiencies demonstrate multigenetic origins of congenital heart disease. *Circ. Res.* **103**, 702–9.

Vitobello, A., Ferretti, E., Lampe, X., Vilain, N., Ducret, S., Ori, M., Spetz, J.-F., Selleri, L. and Rijli, F. M. (2011). Hox and Pbx factors control retinoic acid synthesis during hindbrain segmentation. *Dev. Cell* **20**, 469–82.

Winner, B., Cooper-Kuhn, C. M., Aigner, R., Winkler, J. and Kuhn, H. G. (2002). Long-term survival and cell death of newly generated neurons in the adult rat olfactory bulb. *Eur. J. Neurosci.* **16**, 1681–1689.

Yao, Z., Farr, G. H., Tapscott, S. J. and Maves, L. (2013). Pbx and Prdm1a transcription factors differentially regulate subsets of the fast skeletal muscle program in zebrafish. *Biol. Open* **2**, 546–55.